Result Fusion for Integrated Active and Passive Sensing in DFRC Systems

Wenchao Xia*, Xingliang Lou*, Kai-Kit Wong†, Tony Q. S. Quek‡, and Hongbo Zhu*

***Abstract*—Most existing works on dual-function radar-communication (DFRC) systems mainly focus on active sensing, but ignore passive sensing. To leverage multi-static sensing capability, we explore integrated active and passive sensing (IAPS) in DFRC systems to remedy sensing performance. The multi-antenna base station (BS) is responsible for communication and active sensing by transmitting signals to user equipments while detecting a target according to echo signals. In contrast, passive sensing is performed at the receive access points (RAPs). Considering the limited capacity of backhaul links, the signals received at the RAPs cannot be sent to the central controller (CC) directly. Instead, a novel metric of result aggregation for IAPS is proposed. Specifically, each RAP, as well as the BS, makes decisions independently and sends its binary inference results to the CC for result fusion via voting aggregation. Then, aiming at minimizing the probability of error at the CC under communication quality of service constraints, an algorithm of power optimization is proposed. Finally, numerical results validate the positive effect of dedicated sensing symbols and the potential of the proposed IAPS scheme.**

***Index Terms*—DFRC, integrated active and passive sensing, fusion strategy, voting aggregation, power allocation**

I. Introduction

Communication networks are evolving from 5G to 6G in pursuit of a network that achieves global coverage, green intelligence, sensory interconnection, and synesthesia integration [1]. Electromagnetic wave has the ability to both sense environment and transmit data, but most existing works study and treat these two techniques independently, resulting in a conflict of wireless resources between sensing and communication systems. To improve frequency spectrum and hardware efficiency, researchers are recently considering the function integration of wireless communication and radar sensing, which promotes the research on dual-function radar-communication (DFRC) systems [2].

The primary idea behind DFRC systems is to share infrastructure and resources between communication and sensing functions [3]. Recently, there have been some works [4–6] on the design and performance analysis of DFRC systems. However, only signals of mono-static sensing transceiver was used in [4–6]. To improve sensing accuracy, [7–9] attempted to make use of multiple signals for sensing. In particular, [7] proposed an uplink sensing scheme which jointly processed all measurements from the spatial, temporal, and frequency domains for perceptive mobile networks with asynchronous transceivers. In [8], a base station (BS) working as a mono-static radar receiver was used to estimate angles-of-arrival of targets based on its downlink echo signals and uplink reflected signals from the users. To address the self-interference problem of echo signal caused by the concurrent information transmission, the authors of [9] proposed to select one BS as a receiver to receive the echo signals while other BSs act as transmitters.

Different from the above works which are based on mono-static sensing, multi-static sensing has attracted growing interests and is expected to bring various advantages over the conventional mono-static sensing [10–12]. Multi-static sensing can not only reduce the mono-static sensing uncertainties caused by noise or incompleteness due to wireless fading and interference [13], but also provide better sensing coverage and capture richer sensing information [14]. Despite the above progress, these previous works still suffer from many limitations. On the one hand, although multi-static sensing provides enhanced sensing capability, we note that most existing works focus on active sensing in DFRC systems and ignore the potential performance gain from passive sensing. In multi-static sensing, we refer to the sensing operation based on echo signals as active sensing, whereas the sensing operation based on the received signals from other transmitters (such as BSs and receive access points (RAPs)) as passive sensing. On the other hand, direct transmission of multi-static sensing signals to the central controller (CC) for centralized processing leads to high communication overhead. However, the channel links to the CC are often capacity-limited.

Motivated by the analysis above, we aim to improve sensing performance by integrated active and passive sensing (IAPS) in DFRC systems without sacrificing communication performance. Specifically, the BS is responsible for communication as well as active sensing by transmitting signals to user equipments (UEs) while simultaneously detecting targets according to the echo signals. The RAPs do not transmit signals to UEs but they can process reflected signals by the target. Considering the fact that the capacity of backhaul links between the CC and the RAPs are usually limited, it is hard for each RAP to send its observation (i.e., reflected signals they have received) directly to the CC. This practical consideration poses a challenge on the integration of active and passive sensing. The contributions of this work are summarized as follows:

*Jiangsu Key Laboratory of Wireless Communications, Nanjing University of Posts and Telecommunications, Nanjing 210003, P. R. China, Email: {2022010109, xiawenchao, zhuhb}@njupt.edu.cn

†Department of Electronic and Electrical Engineering, University College London, London WC1E 6BT, UK, Email: kai-kit.wong@ucl.ac.uk

‡Information System Technology and Design Pillar, Singapore University of Technology and Design, Singapore, Email: tonyquek@sutd.edu.sg

This work was supported in part by the National Natural Science Foundation of China (No. 62201285) and in part by the Natural Science Foundation on Frontier Leading Technology Basic Research Project of Jiangsu (No. BK20212001).

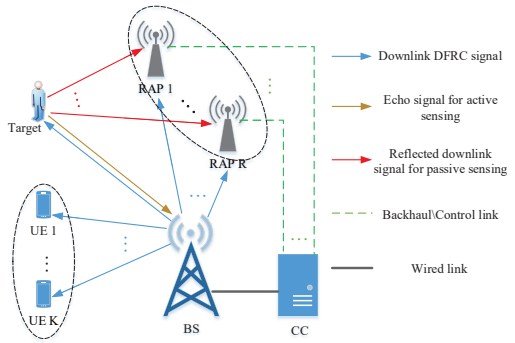

Fig. 1. Illustration of IAPS in DFRC System.

1) We consider a DFRC system where a BS communicates with UEs and senses a target simultaneously. Multiple RAPs are connected to the CC via backhaul links. In addition to active sensing signals received at the BS, passive sensing signals received at the RAPs are also exploited and then the IAPS scheme is proposed to improve sensing performance.
2) Due to limited backhaul capacity, the BS and the RAPs make decisions based on their observation independently and send binary inference results to the CC for result fusion. Upon receiving active and passive sensing binary inference results, the CC performs voting aggregation to determine whether the target exists. We convert the probability of error minimization into a maximization problem of joint detection probability and propose a heuristic power optimization algorithm.
3) Finally, numerical simulations validate the performance gain of the proposed IAPS scheme and the positive effect of dedicated sensing symbols. It also reveals the effectiveness of the proposed fusion schemes. Besides, we find that the overall performance can be improved by increasing the available sensing information from RAPs.

II. System Model

A. System Setting

We consider a downlink DFRC system, as depicted in Fig. 1, where a BS equipped with M transmit antennas and N_0 receive antennas is responsible for serving K single-antenna UEs and detecting a single target simultaneously. There are also R RAPs each with N_1 receive antennas, which can be used to receive the reflected signals for sensing. Here, we refer to the sensing operation at the BS and RAPs as active and passive sensing, respectively. Besides, a CC is introduced to process both the active and passive sensing signals. For notational convenience, we denote the set of UEs and the set of RAPs by $\mathcal{K} = \{1, 2, \ldots, K\}$ and $\mathcal{R} = \{1, 2, \ldots, R\}$, respectively. The BS is indexed using 0 and we denote the set of the BS and RAPs by $\mathcal{R}' = \mathcal{R} \bigcup \{0\}$, Besides, the target is indexed using 0 and the set of UEs and target are denoted by $\mathcal{K}' = \mathcal{K} \bigcup \{0\}$.

We define $\mathbf{s}_0 \in \mathbb{C}^{L\times 1}$ as the dedicated sensing symbol vector and $\mathbf{s}_k \in \mathbb{C}^{L\times 1}$ as the communication symbol vector of the k-th UE, respectively, with L being the length of the communication time slots. It is assumed that the sensing and communication symbols are independent of each other so that $\frac{1}{L}\mathbb{E}(\mathbf{S}\mathbf{S}^H) \approx \mathbf{I}_{K+1}$, where $\mathbf{S} = [\mathbf{s}_0, \mathbf{s}_1, ..., \mathbf{s}_K]^T$, which holds asymptotically for, e.g., white Gaussian signaling. Then, the DFRC signal matrix is given as $\mathbf{X} = \mathbf{W}\mathbf{S}$, where

$$\mathbf{W} = [\sqrt{p_0}\tilde{\mathbf{w}}_0, \sqrt{p_1}\tilde{\mathbf{w}}_1, ..., \sqrt{p_K}\tilde{\mathbf{w}}_K] \in \mathbb{C}^{M\times(K+1)}, \quad (1)$$

where p_k and $\tilde{\mathbf{w}}_k$ are the transmit power and the normalized precoding vector for target and the k-th UE for all $k \in \mathcal{K}'$, respectively, with $\|\tilde{\mathbf{w}}_k\|_2 = 1$.

B. Communication Model

The received signal in the l-th communication symbol at the k-th UE is given as

$$y_k[l] = \mathbf{h}_k^H \sum_{k'=1}^{K} \sqrt{p_{k'}}\tilde{\mathbf{w}}_{k'} s_{k'}[l] + \sqrt{p_0}\mathbf{h}_k^H \tilde{\mathbf{w}}_0 s_0[l] + n_k[l], \quad (2)$$

where $n_k[l] \sim \mathcal{CN}(0, \sigma_{\mathrm{n}}^2)$ denotes the additive Gaussian white noise (AWGN) with zero mean and variance σ_{n}^2 and $\mathbf{h}_k$ denotes the channel between the k-th UE and the BS.

Then, the signal to interference plus noise ratio (SINR) of the k-th UE is given by

$$\gamma_k = \frac{p_k|\mathbf{h}_k^H\tilde{\mathbf{w}}_k|^2}{\sum_{k'=1,k'\neq k}^{K} p_{k'}|\mathbf{h}_k^H\tilde{\mathbf{w}}_{k'}|^2 + p_0|\mathbf{h}_k^H\tilde{\mathbf{w}}_0|^2 + \sigma_{\mathrm{n}}^2}. \quad (3)$$

C. Sensing Model

The BS can sense the target through the echo signal, which is given as

$$\mathbf{z}_0[l] = \alpha_0 \mathbf{b}_0(\theta)\mathbf{a}^H(\theta)\mathbf{X}[l] + \mathbf{n}_0'[l] \in \mathbb{C}^{N_0\times 1}, \quad (4)$$

where $\mathbf{n}_0'[l] \sim \mathcal{CN}(\mathbf{0}, \sigma_{\mathrm{n}}^2\mathbf{I}_{N_0})$ denotes the AWGN vector, $\mathbf{X}[l]$ represents the l-th column of $\mathbf{X}$, $\alpha_0 \sim \mathcal{CN}(0, \sigma_{\mathrm{rcs}}^2)$ is the combined sensing channel gain that includes the path-loss through target and the radar cross section (RCS) of the target [15], and θ is the azimuth angle of target relative to the antenna array at the BS. The transmit and receive steering vectors of the BS are denoted by

$$\mathbf{a}(\cdot) = \left[1, e^{j2\pi\delta\sin(\cdot)}, \ldots, e^{j2\pi(M-1)\delta\sin(\cdot)}\right]^T \in \mathbb{C}^{M\times 1}, \quad (5)$$

$$\mathbf{b}_0(\cdot) = \left[1, e^{j2\pi\delta\sin(\cdot)}, \ldots, e^{j2\pi(N_0-1)\delta\sin(\cdot)}\right]^T \in \mathbb{C}^{N_0\times 1}, \quad (6)$$

respectively, where δ is the spacing between adjacent antennas normalized by wavelength.

When a target is present, the reflected sensing signal received at the r-th RAP for passive sensing is given as

$$\mathbf{z}_r[l] = \alpha_r \mathbf{b}_1(\varphi_r)\mathbf{a}^H(\theta)\mathbf{X}[l] + \mathbf{G}_r\mathbf{X}[l] + \mathbf{n}_r'[l] \in \mathbb{C}^{N_1\times 1}, \quad (7)$$

where $\mathbf{n}_r'[l] \sim \mathcal{CN}(\mathbf{0}, \sigma_{\mathrm{n}}^2\mathbf{I}_{N_1})$ denotes the AWGN vector, $\alpha_r \sim \mathcal{CN}(0, \sigma_{\mathrm{rcs}}^2)$ is the combined sensing channel gain, φ_r is the azimuth angle of target relative to the r-th RAP, $\mathbf{G}_r \in \mathbb{C}^{N_1\times M}$ represents the target-free channel between the

BS and the r-th RAP and is assumed to subject to complex Gaussian distributions, and $\mathbf{b}_1(\cdot)$ is the steering vector of the RAPs similar to $\mathbf{b}_0(\cdot)$.

D. Transmit Precoding Vectors

The transmit precoding is designed based on the regularized zero-forcing (RZF) scheme, i.e., $\tilde{\mathbf{w}}_k = \bar{\mathbf{w}}_k/\|\bar{\mathbf{w}}_k\|_2$ with $\bar{\mathbf{w}}_k = (\mathbf{H}\mathbf{H}^H + \lambda \mathbf{I}_M)^{-1}\mathbf{h}_k$, where $\mathbf{H} = [\mathbf{h}_1, \mathbf{h}_2, ..., \mathbf{h}_K] \in \mathbb{C}^{M\times K}$ and λ is the regularization parameter.

In order to eliminate the interference caused by sensing symbols to the UEs, we employ the zero-forcing radar (ZFR) precoder $\tilde{\mathbf{w}}_0 = \bar{\mathbf{w}}_0/\|\bar{\mathbf{w}}_0\|_2$ [16], where $\bar{\mathbf{w}}_0 = (\mathbf{I}_M - \mathbf{H}\mathbf{H}^H)^{-1}\mathbf{a}(\theta)$.

III. Proposed Power Optimization

The RAPs are connected to the CC through the backhaul channel with the limited capacity. However, it is impractical for the RAPs to send the sensing signal directly due to the large amount of sensing signals. As an alternative solution, each RAP first makes decisions independently and then send binary inference results to the CC for voting aggregation, such that only a few bits are needed to exchange. Moreover, since the BS and RAPs are network infrastructure and belong to network operators, it is reasonable to assume that the BS and RAPs share a public set of random symbols. After the CC selects the sensing and communication symbols from the known symbol set, it sends the indices of the selected symbols to the RAPs. Then, the RAPs determine a matching filter based on the indices.

A. GLRT Detector

The binary hypothesis is described as

$$\begin{cases} \mathcal{H}_0 : \mathbf{z}_r[l] = \mathbf{G}_r\mathbf{X}[l] + \mathbf{n}'_r[l], \\ \mathcal{H}_1 : \mathbf{z}_r[l] = \alpha_r\mathbf{B}_r\mathbf{X}[l] + \mathbf{G}_r\mathbf{X}[l] + \mathbf{n}'_r[l]. \end{cases} \tag{8}$$

where $\mathbf{B}_0 = \mathbf{b}_0(\theta)\mathbf{a}^H(\theta)$ and $\mathbf{B}_r = \mathbf{b}_1(\varphi_r)\mathbf{a}^H(\theta)$. We use the generalized likelihood ratio test (GLRT) detector to solve the unknown parameters α_r, φ_r and θ. In order to consider the sufficient statistic of the received signal, a matching filter (i.e., $\mathbf{S}$) is adopted [17],

$$\tilde{\mathbf{Z}}_r = \frac{1}{\sqrt{L}}\sum_{l=1}^{L}\mathbf{z}_r[l]\mathbf{S}^H[l] = \alpha_r\sqrt{L}\mathbf{B}_r\mathbf{W} + \frac{1}{\sqrt{L}}(\mathbf{G}_r\mathbf{X} + \mathbf{n}'_r)\mathbf{S}^H. \tag{9}$$

Define $\tilde{\mathbf{z}}$ as the vectorization of $\tilde{\mathbf{Z}}$, which is given as

$$\tilde{\mathbf{z}}_r = \mathrm{vec}(\tilde{\mathbf{Z}}_r) = \alpha_r\sqrt{L}\mathrm{vec}(\mathbf{B}_r\mathbf{W}) + \boldsymbol{\varepsilon}_r, \tag{10}$$

where $\boldsymbol{\varepsilon}_r = \frac{1}{\sqrt{L}}\mathrm{vec}\big((\mathbf{G}_r\mathbf{X} + \mathbf{n}'_r)\mathbf{S}^H\big)$ is zero-mean, complex Gaussian distributed, and has the following block covariance matrix [18]:

$$\mathbf{C}_r = \begin{bmatrix} \mathbf{Q}_r + \sigma_{\mathrm{n}}^2\mathbf{I}_{N_1} & & \mathbf{0} \\ & \cdots & \\ \mathbf{0} & & \mathbf{Q}_r + \sigma_{\mathrm{n}}^2\mathbf{I}_{N_1} \end{bmatrix} \in \mathbb{C}^{N_1M\times N_1M}, \tag{11}$$

where $\mathbf{Q}_r = \mathbf{G}_r\hat{\mathbf{W}}\mathbf{G}_r^H$.

Before using the GLRT detector, we apply a whitening filter to $\boldsymbol{\varepsilon}_r$. Specifically, considering that $\mathbf{C}_r$ is a positive-definite Hermitian matrix, the Cherosky decomposition is adopted as $\mathbf{C}_r^{-1} = \mathbf{U}_r\mathbf{U}_r^H$, where $\mathbf{U}_r$ is the lower triangle matrix. Then, $\mathbf{U}_r^H$ is used as the whitening filter in (8),

$$\begin{cases} \mathcal{H}_0 : \tilde{\mathbf{z}}_r = \mathbf{U}_r^H\boldsymbol{\varepsilon}_r, \\ \mathcal{H}_1 : \tilde{\mathbf{z}}_r = \alpha_r\sqrt{L}\mathbf{U}_r^H\mathbf{d}(\varphi_r,\theta) + \mathbf{U}_r^H\boldsymbol{\varepsilon}_r, \end{cases} \tag{12}$$

where $\mathbf{d}(\varphi_r,\theta) = \mathrm{vec}(\mathbf{B}_r\mathbf{W})$. Thus, the corresponding GLRT detector is given by

$$\Delta_r = \frac{\max_{\alpha_r,\varphi_r,\theta} f(\tilde{\mathbf{z}}_r|\alpha_r,\varphi_r,\theta,\mathcal{H}_1)}{f(\tilde{\mathbf{z}}_r|\mathcal{H}_0)} \underset{\mathcal{H}_0}{\overset{\mathcal{H}_1}{\gtrless}} \zeta, \tag{13}$$

where $f(\tilde{\mathbf{z}}_r|\alpha_r,\varphi_r,\theta,\mathcal{H}_1)$ and $f(\tilde{\mathbf{z}}_r|\mathcal{H}_0)$ are the joint probability density function under $\mathcal{H}_1$ and $\mathcal{H}_0$, respectively, and ζ is the decision threshold. For given φ_r and θ, the maximum likelihood estimation (MLE) of α_r is obatined using the complex least-squares estimation and given as

$$\hat{\alpha}_r = \frac{\mathbf{d}^H(\varphi_r,\theta)\mathbf{C}_r^{-1}\tilde{\mathbf{z}}_r}{\mathbf{d}^H(\varphi_r,\theta)\mathbf{C}_r^{-1}\mathbf{d}(\varphi_r,\theta)}. \tag{14}$$

By substituting (14) into (13), the MLE of $[\varphi_r,\theta]$ can be expressed as

$$[\hat{\varphi}_r,\hat{\theta}] = \arg\max_{\varphi_r,\theta}\frac{\left|\mathbf{d}^H(\varphi_r,\theta)\mathbf{C}_r^{-1}\tilde{\mathbf{z}}_r\right|^2}{\mathbf{d}^H(\varphi_r,\theta)\mathbf{C}_r^{-1}\mathbf{d}(\varphi_r,\theta)}. \tag{15}$$

Hence, the GLRT test statistic is expressed as

$$\ln(\Lambda_r) = \frac{\left|\mathrm{tr}(\tilde{\mathbf{Z}}_r\mathbf{W}^H\hat{\mathbf{B}}_r^H\tilde{\mathbf{Q}}_r^{-1})\right|^2}{\mathrm{tr}(\hat{\mathbf{B}}_r\hat{\mathbf{W}}\hat{\mathbf{B}}^H\tilde{\mathbf{Q}}_r^{-1})} \underset{\mathcal{H}_0}{\overset{\mathcal{H}_1}{\gtrless}} \ln(\zeta), \tag{16}$$

where $\tilde{\mathbf{Q}}_r = \mathbf{Q}_r + \sigma_{\mathrm{n}}^2\mathbf{I}_{N_1}$. The asymptotic distribution is expressed as

$$\ln(\Lambda_r) \sim \begin{cases} \mathcal{H}_1 : \mathcal{X}_2^2(\rho_r), \\ \mathcal{H}_0 : \mathcal{X}_2^2, \end{cases} \tag{17}$$

where $\mathcal{X}_2^2$ and $\mathcal{X}_2^2(\rho_r)$ are central and non-central chi-squared distributions with two Degrees of Freedom, respectively, and the non-centrality parameter ρ_r of the r-th RAP is given as

$$\begin{aligned} \rho_r &= \mathbb{E}\big(|\alpha_r|^2L\,\mathrm{vec}^H(\mathbf{B}_r\mathbf{W})\mathbf{C}_r^{-1}\,\mathrm{vec}(\mathbf{B}_r\mathbf{W})\big) \\ &= \sigma_{\mathrm{rcs}}^2L\,\mathrm{tr}\left(\mathbf{B}_r\hat{\mathbf{W}}\mathbf{B}_r^H(\mathbf{Q}_r + \sigma_{\mathrm{n}}^2\mathbf{I}_{N_1})^{-1}\right). \end{aligned} \tag{18}$$

Besides, the non-centrality parameter ρ_0 of the BS is given as

$$\rho_0 = \sigma_{\mathrm{rcs}}^2L\,\mathrm{tr}\left(\mathbf{B}_0\hat{\mathbf{W}}\mathbf{B}_0^H(\sigma_{\mathrm{n}}^2\mathbf{I}_{N_1})^{-1}\right). \tag{19}$$

When the GLRT is used, the threshold ζ can be expressed as $\zeta = \mathfrak{F}_{\mathcal{X}_2^2}^{-1}(1 - P_{\mathrm{FA}})$, and the detection probability P_{D} is given as $P_{\mathrm{D}} = 1 - \mathfrak{F}_{\mathcal{X}_2^2(\rho_r)}(\zeta)$, where $\mathfrak{F}_{\mathcal{X}_2^2(\rho_r)}$ is the non-central chi-square Cumulative Distribution Function [19].

B. Voting Aggregation

The CC performs voting aggregation when receiving the binary inference results from the RAPs and BS, which can be

modeled by

$$\begin{cases}\mathcal{H}_0: \text{ No target,}\\ \mathcal{H}_1: \text{ Exist target.}\end{cases} \tag{20}$$

Then the voting rule is expressed as

$$\begin{cases}\mathcal{H}_0: \sum_{r=0}^{R} D_r \le \kappa,\\ \mathcal{H}_1: \sum_{r=0}^{R} D_r \ge \kappa,\end{cases} \tag{21}$$

where D_r, $r \in \mathcal{R}'$ is the binary inference result, with $D_r = 0$ standing for no target and $D_r = 1$ standing for an existing target, κ represents the voting threshold. The probability of error at the CC is [20]

$$\Upsilon(\kappa, \hat{P}_{\mathrm{D}}) = \frac{1}{2} + \frac{1}{2}\sum_{i=0}^{\kappa-1}\binom{R+1}{i}\times \left[(\hat{P}_{\mathrm{D}})^i(1-\hat{P}_{\mathrm{D}})^{R+1-i} - (\hat{P}_{\mathrm{FA}})^i(1-\hat{P}_{\mathrm{FA}})^{R+1-i}\right], \tag{22}$$

where $\hat{P}_{\mathrm{D}} = \frac{1}{R+1}\sum_{r=0}^{R} P_{\mathrm{D}_r}$ and $\hat{P}_{\mathrm{FA}} = \frac{1}{R+1}\sum_{r=0}^{R} P_{\mathrm{FA}_r}$. P_{D_r} and P_{FA_r},$r \in \mathcal{R}'$ represent the detection probability and the false alarm probability, respectively, and

$$\binom{R+1}{i} = \frac{(R+1)!}{i!(R+1-i)!}. \tag{23}$$

The optimal κ is obtained as [20]

$$\tilde{\kappa} = \min\left(R+1, \left\lceil \frac{R+1}{1+\beta(\hat{P}_{\mathrm{D}})}\right\rceil\right), \tag{24}$$

where

$$\beta(\hat{P}_{\mathrm{D}}) = \frac{\ln\frac{\hat{P}_{\mathrm{FA}}}{\hat{P}_{\mathrm{D}}}}{\ln\frac{1-\hat{P}_{\mathrm{D}}}{1-\hat{P}_{\mathrm{FA}}}}. \tag{25}$$

C. Problem Formulation

We aim to minimize the probability of error at the CC, but the expression of $\Upsilon(\kappa, \hat{P}_{\mathrm{D}})$, as shown in (22), is quite complex. To handle this issue, we first introduce the following lemmas.

Lemma 1: Given $\hat{P}_{\mathrm{D}} \in (0,1)$, $\beta(\hat{P}_{\mathrm{D}})$ decreases as $\hat{P}_{\mathrm{D}}$ increases.

Proof: The proof is based on the first and second derivatives and is omitted here due to the limited space. ■

Lemma 2: Given $\hat{P}_{\mathrm{D}} \in (0,1)$, $\Upsilon(\tilde{\kappa}, \hat{P}_{\mathrm{D}})$ decreases as $\hat{P}_{\mathrm{D}}$ increases.

Proof: Based on **Lemma** 1, $\left\lceil \frac{R+1}{1+\beta(\hat{P}_{\mathrm{D}})}\right\rceil$ follows a stepwise ascent as $\hat{P}_{\mathrm{D}}$ increases. We first define $\hat{P}_{\mathrm{D}}^{\tilde{\kappa},\min}$ and $\hat{P}_{\mathrm{D}}^{\tilde{\kappa},\max}$, which satisfy

$$\hat{P}_{\mathrm{D}}^{\tilde{\kappa},\min} = \arg\min_{\hat{P}_{\mathrm{D}}}\left[\min\left(R+1, \left\lceil \frac{R+1}{1+\beta(\hat{P}_{\mathrm{D}})}\right\rceil\right) = \tilde{\kappa}\right], \tag{26}$$

and

$$\hat{P}_{\mathrm{D}}^{\tilde{\kappa},\max} = \arg\max_{\hat{P}_{\mathrm{D}}}\left[\min\left(R+1, \left\lceil \frac{R+1}{1+\beta(\hat{P}_{\mathrm{D}})}\right\rceil\right) = \tilde{\kappa}\right], \tag{27}$$

respectively. κ is a constant and equal to $\tilde{\kappa}$ when $\hat{P}_{\mathrm{D}} \in [\hat{P}_{\mathrm{D}}^{\kappa,\tilde{\min}}, \hat{P}_{\mathrm{D}}^{\kappa,\tilde{\max}}]$. We will prove **Lemma** 2 in two steps. Specifically, we first prove that the probability of error $\Upsilon\left(\kappa, \hat{P}_{\mathrm{D}}\right)$ at the CC decreases as $\hat{P}_{\mathrm{D}}$ increases when $\hat{P}_{\mathrm{D}}^{\tilde{\kappa}} \in (\hat{P}_{\mathrm{D}_{\min}}^{\tilde{\kappa}}, \hat{P}_{\mathrm{D}_{\max}}^{\tilde{\kappa}}]$. In such a case, $\tilde{\kappa}$ is fixed and equal to $\tilde{\kappa}$ and $\Upsilon(\kappa, \hat{P}_{\mathrm{D}})$ can be simplified as

$$\Upsilon_1(\hat{P}_{\mathrm{D}}) = \frac{1}{2}\sum_{i=0}^{\tilde{\kappa}-1}\binom{R+1}{i}(\hat{P}_{\mathrm{D}})^i(1-\hat{P}_{\mathrm{D}})^{R+1-i}, \tag{28}$$

which decreases as $\hat{P}_{\mathrm{D}}$ increases. This is because the CDF of the binomial distribution $\Upsilon_1(\hat{P}_{\mathrm{D}})$ can be represented in terms of the regularized incomplete beta function [21]:

$$\Upsilon(\hat{P}_{\mathrm{D}}) = (R+2-\tilde{\kappa})\binom{R+1}{i}\int_0^{1-\hat{P}_{\mathrm{D}}} t^{R+1-\tilde{\kappa}}(1-t)^{\tilde{\kappa}-1}\mathrm{d}t,$$

whose derivative meets the following constraint,

$$\frac{\mathrm{d}\Upsilon(\hat{P}_{\mathrm{D}})}{\mathrm{d}\hat{P}_{\mathrm{D}}} = -(R+2-\tilde{\kappa})\binom{R+1}{i}(1-\hat{P}_{\mathrm{D}})^{R+1-\tilde{\kappa}}(\hat{P}_{\mathrm{D}})^{\tilde{\kappa}-1} \le 0.$$

Secondly, we prove that the probability of error $\Upsilon(\kappa, \hat{P}_{\mathrm{D}})$ at the CC decreases when κ varies from $\tilde{\kappa}$ to $\tilde{\kappa}+1$ due to the increase of $\hat{P}_{\mathrm{D}}$. According to (26) and (27), we have

$$\begin{aligned}&\Upsilon(\tilde{\kappa}+1, \hat{P}_{\mathrm{D}}^{\tilde{\kappa}+1,\min}) - \Upsilon(\tilde{\kappa}, \hat{P}_{\mathrm{D}}^{\tilde{\kappa},\max})\\ &\le \binom{R+1}{\tilde{\kappa}}\left[(\hat{P}_{\mathrm{D}}^{\tilde{\kappa},\max})^{\tilde{\kappa}}(1-\hat{P}_{\mathrm{D}}^{\tilde{\kappa},\max})^{R+1-\tilde{\kappa}}\right.\\ &\quad \left. - (\hat{P}_{\mathrm{FA}})^{\tilde{\kappa}}(1-\hat{P}_{\mathrm{FA}})^{R+1-\tilde{\kappa}}\right],\end{aligned} \tag{29}$$

and

$$\tilde{\kappa} = \frac{R+1}{1+\beta(\hat{P}_{\mathrm{D}}^{\tilde{\kappa},\max})} = \frac{(R+1)\ln\frac{1-\hat{P}_{\mathrm{FA}}}{1-\hat{P}_{\mathrm{D}}^{\tilde{\kappa},\max}}}{\ln\frac{\hat{P}_{\mathrm{D}}^{\tilde{\kappa},\max}(1-\hat{P}_{\mathrm{FA}})}{\hat{P}_{\mathrm{FA}}(1-\hat{P}_{\mathrm{D}}^{\tilde{\kappa},\max})}}. \tag{30}$$

Then, substituting (30) into (29), we obtain

$$\Upsilon(\tilde{\kappa}+1, \hat{P}_{\mathrm{D}}^{\tilde{\kappa},\max}) - \Upsilon(\tilde{\kappa}, \hat{P}_{\mathrm{D}}^{\tilde{\kappa},\max}) = 0 \tag{31}$$

which suggests that $\Upsilon(\kappa, \hat{P}_{\mathrm{D}})$ decreases when κ varies from $\tilde{\kappa}$ to $\tilde{\kappa}+1$. Finally, we can conclude that $\Upsilon(\kappa, \hat{P}_{\mathrm{D}})$ decreases as $\hat{P}_{\mathrm{D}}$ increases in the whole feasible region $\hat{P}_{\mathrm{D}} \in (0,1)$. ■

Based on **Lemma** 2, the minimization of the probability of error at the CC is equivalent to the maximization of $\hat{P}_{\mathrm{D}}$. Thus, the optimization problem is formulated as

$$\begin{aligned}\mathcal{P}_1: &\max_{\mathbf{p}\ge\mathbf{0}} \hat{P}_{\mathrm{D}}\\ &\text{s.t. } \gamma_k \ge \Gamma, k \in \mathcal{K},\\ &||\mathbf{p}||_1 = P_{\max},\end{aligned}$$

which is a non-convex problem. Before giving the solution to problem $\mathcal{P}_1$, we first introduce the following lemma.

Lemma 3: When p_0 gradually increases and satisfies the transmit power constraint $||\mathbf{p}||_1 = P_{\max}$, $\hat{P}_{\mathrm{D}}$ gradually increases.

Proof: Since $\hat{P}_{\mathrm{D}}$ is the average of P_{D_r} and P_{D_r} is a monotonically increasing function with respect to ρ_r, we just need to prove that ρ_r increases as p_0 increases. It is observed that $\mathrm{tr}(\mathbf{Q}_r + \sigma_{\mathrm{n}}^2\mathbf{I}_{N_1})$ is a constant associated with $P_{\max}$, and

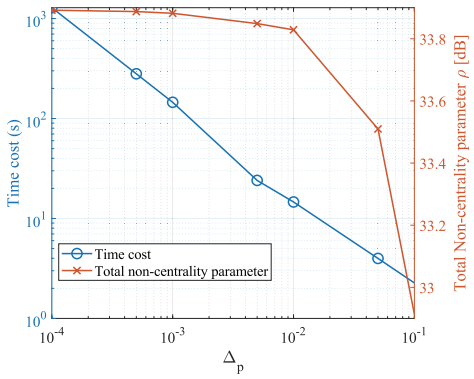

Fig. 2. The trade-off between the step size Δ_p and the time cost or the sensing performance.

we also have

$$\begin{aligned}\mathrm{tr}(\mathbf{B}_r\hat{\mathbf{W}}\mathbf{B}_r^H) &= \mathrm{tr}\left(\hat{\mathbf{W}}\mathbf{a}(\theta)\mathbf{b}_1^H(\varphi_r)\mathbf{b}_1(\varphi_r)\mathbf{a}^H(\theta)\right)\\ &\simeq \mathrm{tr}\left(\hat{\mathbf{W}}\mathbf{a}(\theta)\mathbf{a}^H(\theta)\right).\end{aligned} \tag{32}$$

where $\simeq$ represents the same trend with respect to the variation of p_0 on the left-hand and right-hand sides.

Then,

$$\rho_r \simeq \mathrm{tr}\left(\mathbf{B}_r\hat{\mathbf{W}}\mathbf{B}_r^H\right) = \mathrm{tr}\left(\mathrm{diag}(\mathbf{p})\tilde{\mathbf{W}}^H\mathbf{a}(\theta)\mathbf{a}^H(\theta)\tilde{\mathbf{W}}\right). \tag{33}$$

Obviously, $\tilde{\mathbf{w}}_0^H\mathbf{a}(\theta) > \tilde{\mathbf{w}}_i^H\mathbf{a}(\theta)$ due to the ZFR precoder. Thus, ρ_r increases as p_0 increases. ■

Based on **Lemma** 3, we propose a heuristic algorithm and summarize the proposed algorithm in Algorithm 1. Specifically, the gap between the performance achieved by the heuristic algorithms and the optimal (upper bound) performance is mainly caused by Δp. When Δp is small enough, the heuristic algorithm performance is equal to the optimal performance but the running time is very long. Fig. 2 shows that the trade-off between the step size Δ_p and the time cost or the sensing performance. Taking into account the time cost and sensing performance, we set Δ_p to 0.01.

Algorithm 1 Proposed heuristic algorithm of power allocation.

1: Initialize $p_0' = P_{\max}$, the step size Δp, and $P_{\mathrm{sum}} = p_0'$.
2: **while** $P_{\mathrm{sum}} >= P_{\max}$ **do**
3: Set $p_0 = p_0' - \Delta p$.
4: Find solution to the following problem using semi-definite programming (SDP), i.e.,

$$\mathcal{P}_{\mathrm{A}}: \begin{cases}\min_{\mathbf{p}'} & \|\mathbf{p}\|_1\\ \text{s.t.} & \gamma_k \geq \Gamma, \quad k \in \mathcal{K}.\end{cases}$$

5: Set $P_{\mathrm{sum}} = \|\mathbf{p}\|_1$.
6: Set $p_0' = p_0$.
7: **end while**
8: Output: $\mathbf{p}$.

D. Complexity Analysis

Note that the complexity of Algorithm 1 is mainly determined by finding solution to $\mathcal{P}_{\mathrm{A}}$ using SDP, which needs to be done by each iteration. The corresponding SDP problem has K nonnegative variables and K linear inequality constraints. For a feasible instance of $\mathcal{P}_{\mathrm{A}}$, interior point methods can generate an μ-optimal solution in $\mathcal{O}(\sqrt{K}\log(1/\mu))$ iterations, each requiring at most $\mathcal{O}(K^3)$ arithmetic operations. Then we set the complexity of solving $\mathcal{P}_{\mathrm{A}}$ as $\mathcal{O}(D)$. Hence, the complexity for Algorithm 1 is $\mathcal{O}(D_{\mathrm{iter}}D)$, where D_{iter} is the number of iterations, which is known to have the order of magnitude of $\mathcal{O}(\log(P_{\max}/\Delta p))$.

IV. Numerical Results

To evaluate the performance of the proposed DFRC system, we perform numerical simulations in a 500 m $\times$ 500 m region with a BS, $R = 10$ RAPs, and $K = 8$ UEs in the suburb area. We assume that the target is dynamic, in which the velocity of the target is low compared to the total sensing duration. However, in order to facilitate simulation, the locations of the RAPs, UEs, and BS are randomly generated and the target is in the center of the region. The BS and RAPs each is equipped with $N_0 = N_1 = 20$ receive antennas. Besides, the BS is equipped with $M = 16$ transmit antennas [10]. The channel model is generated using $\mathbf{h}_k = \sqrt{m_k}\tilde{\mathbf{h}}_k \in \mathbb{C}^{M\times 1}$, where $\tilde{\mathbf{h}}_k \sim \mathcal{CN}(\mathbf{0}, \mathbf{I}_M)$ is the small-scale fading and $m_k = 128.1 + 37.6\log_{10}(d)$ [dB] represents the path loss between the k-th UE and BS with d being the distance in kilometers. The target-free channel $\mathbf{G}$ is generated using the same channel model. The combined sensing channel gain of target is using the Swerling-I model. The symbol number is set as $L = 30$ and the detection threshold is determined by the false alarm probability $P_{\mathrm{FA}} = 10^{-5}$. The SINR threshold is set as $\Gamma = 15$ dB.

Before presenting the numerical results, we first introduce the following baseline schemes for comparison. Firstly, we find the solution to problem $\mathcal{P}_1$ considering the cases with and without dedicated sensing symbols (marked as "with s_0" and "w/o s_0", respectively). Then, only-active and only-passive sensing schemes (marked as "active" and "passive", respectively) are introduced.

We evaluate these schemes using average detection probability, which is calculated by averaging over 1000 random samples. Fig. 3 shows that the average detection probability increases with the increase of σ_{rcs}^2. It is observed that the proposed IAPS scheme always achieves a higher average detection probability than that of the only-active and only-passive sensing schemes. We also observe that compared to the cases without dedicated sensing symbols, the average detection probability of difference schemes can be improved by using dedicated sensing symbols, which validates the importance of dedicated sensing symbols. Moreover, the performance of the only-passive sensing scheme is much better than that of the only-active sensing scheme. This is because R binary inference results can be utilized in the only-passive sensing scheme.

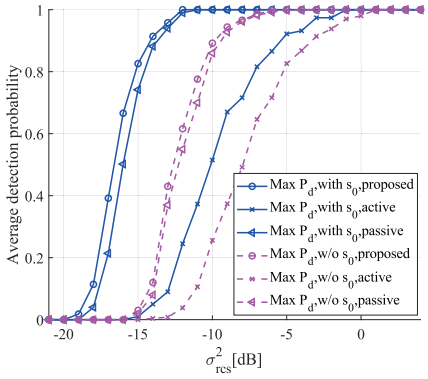

Fig. 3. The average detection probability vs. σ^2_{rcs}, $P_{\max} = 30$ dBm.

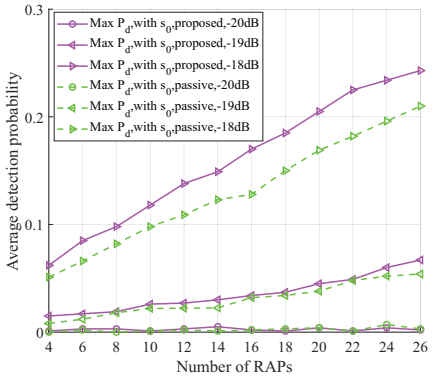

Fig. 4. The average detection probability vs. the number of RAPs, $P_{\max} = 30$ dBm.

However, only one binary inference result is utilized in the only-active sensing scheme.

Fig. 4 shows the average detection probability with respect to the number of RAPs with different σ^2_{rcs} values. The increase of the RAP number can reduce the probability of misjudgment after the voting aggregation. We note that the average detection probability increases as the number of the RAPs increases when $\sigma^2_{\text{rcs}} \geq -19$ dB, but the curve with $\sigma^2_{\text{rcs}} = -18$dB rises faster than the curve with $\sigma^2_{\text{rcs}} = -19$dB. In addition, we also find that when $\sigma^2_{\text{rcs}} = -20$dB, the average detection probability is almost unchanged. This is because the voting aggregation at the CC highly depends on the binary inference results of each single RAP and the detection probability of each single RAP relies on σ^2_{rcs}.

V. CONCLUSION

In this paper, we considered a DFRC systems where a multi-antenna BS is responsible for communication and active sensing and multiple RAPs perform passive sensing. Due to limited backhaul capacity, a novel metric of result aggregation for IAPS is proposed. In particular, the BS and RAPs make decisions independently and send binary inference results to the CC for result fusion via voting aggregation. We then formulated optimization problem to minimize the probability of error at the CC under communication QoS constraints and proposed a heuristic power optimization algorithm. Finally, numerical results validated the positive effect of dedicated sensing symbols and the performance gain of the proposed IAPS scheme.

REFERENCES

[1] Z. Zhang, Y. Xiao, Z. Ma, M. Xiao, Z. Ding, X. Lei, G. K. Karagiannidis, and P. Fan, "6G wireless networks: Vision, requirements, architecture, and key technologies," *IEEE Trans. Veh. Technol.*, vol. 14, no. 3, pp. 28–41, July 2019.

[2] F. Liu, C. Masouros, A. P. Petropulu, H. Griffiths, and L. Hanzo, "Joint radar and communication design: Applications, state-of-the-art, and the road ahead," *IEEE Trans. Commun.*, vol. 68, no. 6, pp. 3834–3862, Jun. 2020.

[3] J. A. Zhang, M. L. Rahman, K. Wu, X. Huang, Y. J. Guo, S. Chen, and J. Yuan, "Enabling joint communication and radar sensing in mobile networks-A survey," *IEEE Commun. Surveys Tuts.*, vol. 24, no. 1, pp. 306–345, Feb. 2022.

[4] F. Liu, Y.-F. Liu, A. Li, C. Masouros, and Y. C. Eldar, "Cramér-rao bound optimization for joint radar-communication beamforming," *IEEE Trans. Signal Process.*, vol. 70, pp. 240–253, Feb. 2022.

[5] T. Guo, X. Li, M. Mei, Z. Yang, J. Shi, K.-K. Wong, and Z. Zhang, "Joint communication and sensing design in coal mine safety monitoring: 3D phase beamforming for ris-assisted wireless networks," *IEEE Internet Things*, pp. 1–1, Feb. 2023.

[6] G. Li, S. Wang, J. Li, R. Wang, F. Liu, X. Peng, T. X. Han, and C. Xu, "Integrated sensing and communication from learning perspective: An sdp3 approach," *IEEE Internet Things*, pp. 1–1, Aug. 2023.

[7] Z. Ni, J. A. Zhang, X. Huang, K. Yang, and J. Yuan, "Uplink sensing in perceptive mobile networks with asynchronous transceivers," *IEEE Trans. Signal Process.*, vol. 69, pp. 1287–1300, Feb. 2021.

[8] A. Chowdary, A. Bazzi, and M. Chafii, "On hybrid radar fusion for integrated sensing and communication," *arXiv preprint arXiv:2303.05722*, 2023.

[9] D. Xu, C. Liu, S. Song, and D. W. K. Ng, "Integrated sensing and communication in coordinated cellular networks," *arXiv preprint arXiv:2305.01213*, 2023.

[10] Z. Behdad, Ö. T. Demir, K. W. Sung, E. Björnson, and C. Cavdar, "Power allocation for joint communication and sensing in cell-free massive mimo," in *Proc. IEEE Global Commun. Conf. (GLOBECOM), Anaheim, Rio de Janeiro, Brazil*, Dec. 2022, pp. 4081–4086.

[11] V. Yajnanarayana and H. Wymeersch, "Multistatic sensing of passive targets using 6G cellular infrastructure," *arXiv preprint arXiv:2211.05340*, 2022.

[12] G. Li, S. Wang, K. Ye, M. Wen, D. W. K. Ng, and M. Di Renzo, "Multi-point integrated sensing and communication: Fusion model and functionality selection," *IEEE Wireless Commun. Lett.*, vol. 11, no. 12, pp. 2660–2664, Dec. 2022.

[13] S. Z. Gurbuz and M. G. Amin, "Radar-based human-motion recognition with deep learning: Promising applications for indoor monitoring," *IEEE Signal Process. Mag.*, vol. 36, no. 4, pp. 16–28, July 2019.

[14] H. Godrich, A. M. Haimovich, and R. S. Blum, "Target localization accuracy gain in mimo radar-based systems," *IEEE Trans. Inf. Theory*, vol. 56, no. 6, pp. 2783–2803, June 2010.

[15] N. Zhao, Y. Wang, Z. Zhang, Q. Chang, and Y. Shen, "Joint transmit and receive beamforming design for integrated sensing and communication," *IEEE Commun. Lett.*, vol. 26, no. 3, pp. 662–666, Mar. 2022.

[16] S. Buzzi, C. D' Andrea, and M. Lops, "Using massive MIMO arrays for joint communication and sensing," in *Proc. IEEE Asilomar Conf. Signals, Syst., Comput., Pacific Grove, CA, USA*, 2019, pp. 5–9.

[17] A. Khawar, A. Abdelhadi, and C. Clancy, "Target detection performance of spectrum sharing MIMO radars," *IEEE Sensors J.*, vol. 15, no. 9, pp. 4928–4940, Sep. 2015.

[18] F. Liu, C. Masouros, A. Li, T. Ratnarajah, and J. Zhou, "MIMO radar and cellular coexistence: A power-efficient approach enabled by interference exploitation," *IEEE Trans. Signal Process.*, vol. 66, no. 14, pp. 3681–3695, July 2018.

[19] I. Bekkerman and J. Tabrikian, "Target detection and localization using MIMO radars and sonars," *IEEE Trans. Signal Process.*, vol. 54, no. 10, pp. 3873–3883, Oct 2006.

[20] P. K. Varshney, *Distributed Detection and Data Fusion*. New York: Springer-Verlag, 1997.

[21] G. P. Wadsworth, J. G. Bryan, and A. C. Eringen, "Introduction to probability and random variables," *J. Appl. Mech.*, vol. 87, no. 2, pp. 271–272, 1961.